

**MODELING THE EFFECT OF TEMPERATURE-INDUCED
SURFACE-TENSION GRADIENT IN COATING PROCESSES**

by

Bawadi Abdullah

Submitted
in partial fulfillment of the requirements
for the degree of

MASTER OF ENGINEERING

Major Subject: Chemical Engineering

at

DALHOUSIE UNIVERSITY

Halifax, Nova Scotia

November, 2002

©Copyright by Bawadi Abdullah, 2002

Dalhousie University
Faculty of Engineering

Department of Chemical Engineering

The undersigned hereby certify that they have examined, and recommend to the Faculty of Graduate Studies for acceptance, the thesis entitled "Modeling the Effect of Temperature-induced Surface-tension Gradient in Coating Processes" by Bawadi Abdullah in partial fulfillment of the requirements for the degree of Master of Engineering

Dated: Nov. 27/02

Supervisor:

Yuet Pak K. Yuet
Dr. Pak K. Yuet

Examiners:

Mort Fels
Dr. Mort Fels

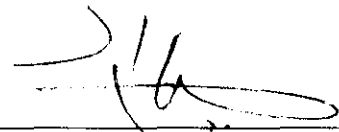
Rafiqul Islam
Dr. Rafiqul Islam

Dalhousie University
Faculty of Engineering

DATE: NOV 28, 2002

AUTHOR: Bawadi Abdullah
TITLE: Modeling the Effect of Temperature-induced Surface-tension Gradient in Coating Processes
MAJOR SUBJECT: Chemical Engineering
DEGREE: Master of Engineering
CONVOCATION: May, 2003

Permission is herewith granted to Dalhousie University to circulate and to have copied for non-commercial purposes, at its discretion, the above thesis upon the request of individuals or institutions.



Signature of Author

The author reserves other publication rights, and neither the thesis nor extensive extracts from it may be printed or otherwise reproduced without the author's written permission.

The author attests that permission has been obtained for the use of any copyright material appearing in this project (other than brief excerpts requiring only proper acknowledgement in scholarly writing), and that all such use is clearly acknowledged.

TABLE OF CONTENTS

TABLES OF CONTENTS	iv
LIST OF TABLES.....	v
LIST OF FIGURES.....	vi
NOMENCLATURE	vii
ACKNOWLEDGEMENTS	ix
ABSTRACT	x
1. INTRODUCTION.....	1
2. LITERATURE REVIEW.....	3
3. MATHEMATICAL MODEL AND NUMERICAL IMPLEMENTATION.....	6
3.1 MODEL DERIVATION	6
3.2 DIMENSIONLESS MODEL	11
3.3 DERIVATION OF DISCRETISATION EQUATIONS	14
4. SIMULATION RESULTS AND DATA ANALYSIS	17
4.1 BASE CASE.....	17
4.1.1 <i>Base Case Results</i>	
4.1.2 <i>Flux Analysis</i>	
4.1.3 <i>Data Analysis</i>	
4.2 EFFECT OF EVAPORATION RATE	23
4.3 EFFECT OF VISCOSITY	25
4.4 EFFECT OF TEMPERATURE.....	27
4.5 EFFECT OF SURFACE TENSION.....	28
4.6 DISCUSSION.....	29
5. CONCLUSIONS	31
6. MODEL LIMITATION AND FUTURE WORKS	33
6.1 MODEL LIMITATIONS	33
6.2 FUTURE WORKS	34
REFERENCES	35

LIST OF TABLES

3.1	Base properties of the coating used for simulation	12
-----	--	----

LIST OF FIGURES

Figure 3.1:	The coating profile on a flat substrate.....	7
Figure 3.2:	The physical situation described by the model.	7
Figure 4.1:	Temperature distribution over dimensionless axial x -direction.....	18
Figure 4.2:	Time variation of dimensionless coating thickness.	18
Figure 4.3:	Distribution of fluxes due to surface-tension gradient (Q_{stg}) and pressure gradient (Q_{pg})	19
Figure 4.4	Flux due to pressure gradient.....	20
Figure 4.5	Dimensionless pressure distributions at free surface in different time.	21
Figure 4.6	Variation of peak height and peak location.	21
Figure 4.7	The peak and trough variances at different times.	22
Figure 4.8	Temperature profile used in studying defect spreading.....	23
Figure 4.9	Coating thickness profile at $t = 200$ s, effect of evaporation rate.	24
Figure 4.10	Evaporation rate profiles. Evaporation rate increases with the dimensionless x -direction until its reaches $x \approx 3.5$	24
Figure 4.11	Coating thickness profiles at $t = 10$ s showing the effect of viscosity.....	25
Figure 4.12	The linear relation between defect formation time and viscosity.	26
Figure 4.13	Defect growth behaviour at different viscosities.	26
Figure 4.14	Temperature profile studying the effect of temperature gradient.	27
Figure 4.15	Effect of temperature gradient on coating thickness at $t = 10$ s.....	28
Figure 4.16	Effect of surface tension on coating thickness.....	29

NOMENCLATURE

H	Initial film thickness, μm
L	Horizontal length scale, cm
T	Temperature, $^{\circ}\text{C}$
\bar{t}	Reference time, s
Δt	Time step size
Δx	Grid size
E	Dimensionless evaporation rate
$e(T)$	Evaporation rate, cm/s
e_0	Reference evaporation rate, cm/s
x	Distance along the substrate, cm
t	Time, s
z	Direction perpendicular to the substrate
h	Coating thickness, cm
A	Dimensionless aspect ratio
Q	Dimensionless total flux
Q_{stg}	Dimensionless flux due to surface tension gradient
Q_{pg}	Dimensionless flux due to pressure gradient
u	Fluid velocity, cm/s
T_c	Critical temperature of pure liquid, $^{\circ}\text{C}$
P_0	Reference pressure, dyne/cm^2

P	Pressure at free surface, dyne/cm ²
n	exponential index

Greek symbol

$\sigma(T)$	Surface tension, dyne/cm
σ_0	Reference surface tension, dyne/cm
σ_∞	Minimum surface tension, dyne/cm
μ_0	Initial coating viscosity, Poise
$\mu(T)$	Coating viscosity, Poise

ACKNOWLEDGEMENTS

First I would like to express my gratitude to my respected supervisor, Dr. Pak K. Yuet, Assistant Professor, Department of Chemical Engineering, for his extensive help and constant guidance, coherent efforts, and advice, without which I could not be able to make progress and overcome many difficulties that I was facing during my work. It was through his assistance and support that I finally completed my project.

It is a great pleasure and proud privilege for me to express my heartiest thanks and gratefulness to Dr. Mort Fels of Chemical Engineering Department, and Dr. Rafiqul Islam of the Department of Civil Engineering, as they kindly agreed to be in my guiding committee.

I would also like to thank my family members and friends, who, through their understanding and constant encouragement, made this work successful.

Finally, I would also like to thank Universiti Teknologi Petronas, Malaysia for funding my study at Dalhousie University.

ABSTRACT

In the application of fluorescent lamp coating, clip marks formed during drying can adversely affect product quality, resulting in higher production cost and/or lower customer satisfaction. It is believed that these defects are caused by gradient in coating surface tension but their mechanisms are still not well understood.

To facilitate a more systematic approach to coatings design, it is important to have a better understanding of the roles of surface tension in defect formation. A one-dimensional mathematical model, which describes the flow of drying coating on horizontal planar substrates, was developed in this study to investigate the formation of defects, particularly in the fluorescent-lamp coating process. A partial differential equation was derived based on the Navier-Stokes equation, using the lubrication approximation for thin layers. The effect of temperature distribution on surface-tension gradient was incorporated into the model, which enhances our ability to quantify defect formation in drying coatings.

The results show that, temperature-induced surface-tension gradient plays a major role in defect formation. The effect of pressure gradient is negligible compared to the surface-tension gradient in defect formation. A linear relation is observed between defect peak growth and time between $t = 10$ s and $t = 500$ s. Defect formation time also varies linearly with viscosity in the range between $\mu = 0.1$ P to 2 P. Parametric studies show that all the parameters studied have an effect on the defect. Temperature shows the greatest influence in defect formation, followed by viscosity. This model can be used as a process analysis tool in industrial applications.

Chapter 1

INTRODUCTION

Many natural phenomena and industrial processes involve the flow of thin liquid films. Examples from the natural world include the airway and alveoli of the lung and cornea of the eye, which are coated with thin liquid lining as a barrier between the air and living tissues. In industry its applications include pharmaceuticals, lubricants, adhesives, dyes, masonry treatments, and glazes. But perhaps the most widespread industrial application is the coating of solid surfaces with paint films. The purposes of coating are to protect, preserve, and beautify the objects to which they are applied. In the United States alone, the sale of paint and coating exceeds billions of dollar each year [1].

Coatings are typically divided into “solvent-based” and “aqueous” coatings. Solvent-based coatings are generally organic, non-aqueous coating, while aqueous coatings use water as the vehicle for other components (e.g. pigment and binder). A decade ago, solvent-based coatings were found to have adverse effects on environment and human health. To avoid these issues, the use of aqueous coatings has increased significantly. This shift is important because water, due to its higher surface tension, is more susceptible to surface-tension-related defect formation. Normally, surfactant is introduced to lower surface tension and enhances wettability. Surfactants can cause substantial change in surface tension when present in low concentrations [3]. Besides surfactant, temperature also has a significant effect on surface tension. The surface tension of a liquid generally decreases as temperature increases, and it becomes very small at temperatures just below the critical temperature [4]. When temperature reaches its critical value, surface tension becomes zero.

Surface-tension gradients can be caused by non-uniform distribution of surfactant, temperature gradient, or concentration gradient between two components (e.g. solvent and resin). The effect of a surface-tension gradient plays a major role in coating processes. For example, in the fluorescent lamp industry, a coating defect, known as “dark line,” is often formed during the drying process. This type of defect is presumably caused by the surface-tension gradient induced by temperature difference that may have developed under the clamps that hold the lamp during drying.

Although it is recognized that surface-tension gradient is a major cause of defect formation, the mechanisms involved are still not well understood. Consequently, defects in industrial coatings are often rectified by trial and error, which is costly and time-consuming. Motivated by this potential application in fluorescent lamp industry, a mathematical model based on lubrication theory is developed in which the defect is produced by a temperature-induced surface-tension gradient. The one-dimensional rectangular geometry model is developed based on the Navier-Stokes equation. The resultant flow equation is discretised and solved numerically. Through a series of parametric studies, we can gain insight into the mechanisms of defect formation.

The objective of this study is to develop a simple but adequate model for analysing the process and enhancing our understanding of defect formation. The parametric studies conducted include the effects of different coating viscosities and temperature profiles. It is expected that the results of these studies can be readily utilised to minimise or eliminate coating defect in industrial applications.

Chapter 2

LITERATURE REVIEW

Many investigators have been interested in studying the effects of surface-tension gradient on coating processes. These efforts have been driven mainly by the coating industry's desire to eliminate or reduce the number of defects created during the coating process. Coating defects cost the coating industry millions of dollar each year and significant resources have been expended to overcoming the problem. For example, in the automobile industry, even a few dozen craters formed during the coating of car bodies can halt production [5].

In mid 1980s, Overdiep [6] investigated the leveling behaviour of solvent-based alkyd paints. He found that Orchard's equation (one of the earliest theoretical analyses of surface leveling) failed to give a qualitative description of the leveling process in his experiments. His experimental results indicated that, in the course of leveling, an initially sinusoidal profile would become horizontal, after which regions that were initially crests would become troughs and vice-versa. He attributed this behaviour to the exclusion of surface-tension gradient effects.

Eres et al. [7] investigated the effects of surface-tension gradient on multicomponent fluid. They found that the surface-tension gradient caused by compositional changes in coating fluid has a significant effect on flow history. For example, surface-tension gradient may cause irregularities in the final dry coating profile when the spatial evaporation gradient acts on the initially uniform coatings. They also found that the oscillatory motion of free surface was created by surface-tension gradient induced by solvent evaporation.

Evans et al. [8] investigated the mechanisms of crater formation. They developed a mathematical model which incorporates the effect of surfactant-induced surface-tension gradient. They found that drying rate and viscosity have significant effects on the crater formation, and crater growth can be minimised by increasing the coating viscosity and lowering the drying rate. The extent of cratering can also be lowered if there is a pre-existing layer of surfactant on the coating surface.

Charles et al. [9] investigated the spreading of a liquid in the presence of surface-tension gradient. Liquid polydimethylsiloxane (PDMS) was spread on a smooth glass plate, which was in direct contact with an open reservoir containing cyclohexane or hexane. They observed that the PDMS spontaneously spread over the glass substrate in cyclohexane but retracted initially before spreading in hexane vapour. These phenomena occur because of the surface-tension difference between cyclohexane and hexane. The surface tension of cyclohexane is higher than that of PDMS, whereas the surface tension of hexane is lower than that of PDMS.

Modeling of surface-tension gradient-driven flow has applications beyond the coating industry. For example, in welding pools containing molten metal, altered surface-tension gradient in the presence of impurities also creates defects [10]. Oreper and Zacharia [11,12] also performed numerical modeling to study the effects of temperature and composition variation on surface-tension gradients. They found good agreement between experimental and numerical results.

Lei et al. [13] investigated the influence of Marangoni flow and evaporation on surface temperature and molten pool shape in laser surface remelting. They found that the laser-induced alloying element vaporization (Langmuir vaporization) heat loss can significantly reduce the surface peak temperature if the temperature variation of surface tension was small. However, when vaporization and Marangoni flow were both present

at the same time, the free surface temperature distribution and its peaks were affected by the surface-tension gradients.

Blunk and Wilkes [14,15] investigated the formation of bondline readout (BLRO) on the polymeric automotive body panels with high-glamor clearcoats coating. BLRO is a coating defect frequently exhibited on the adhesively-bonded sheet molding compound. The formation of BLRO is mainly due to surface-tension gradient induced by temperature and concentration gradients, whereas the pressure gradient works as the leveling force that lower the BLRO formation. The numerical and experimental results obtained were in good agreement.

Chapter 3

MATHEMATICAL MODEL AND NUMERICAL IMPLEMENTATION

A mathematical model based on the Navier-Stokes equation is developed in this study to investigate the effect of temperature-induced surface-tension gradient on coating defection formation. A major advantage of mathematical modeling is that it can provide detailed information not attainable by experiments. For example, in this study the flux distribution can be easily determined numerically whereas it is impossible to measure experimentally. However, it should be noted that experimental investigation is crucial in validating the accuracy of mathematical models.

3.1 Model Derivation

The derivation described below follows closely that in ref. [8]. Basically, we are interested in modeling the behaviour of thin coating layer when it is subjected to an imposed temperature distribution at the surface. Real coatings are complex multi-component mixtures; however, for simplicity, the coating is assumed to be a pure liquid without surfactant in this study. The coating thickness is denoted by $h(x,t)$ as depicted in Figure 3.1, where x is the axial distance measured along the substrate from the center of the disturbance and t is time. The coordinate perpendicular to the substrate is denoted by z . The characteristic coating thickness is H , while L is a substrate length scale. The effect of gravity is neglected in this study, so the pressure at the coating surface depends only on the local surface tension, σ , and the free surface curvature.

The physical situation described by this model is depicted in Figure 3.2. Hot air is blowing on top of the coating surface, and temperature variation is caused by the

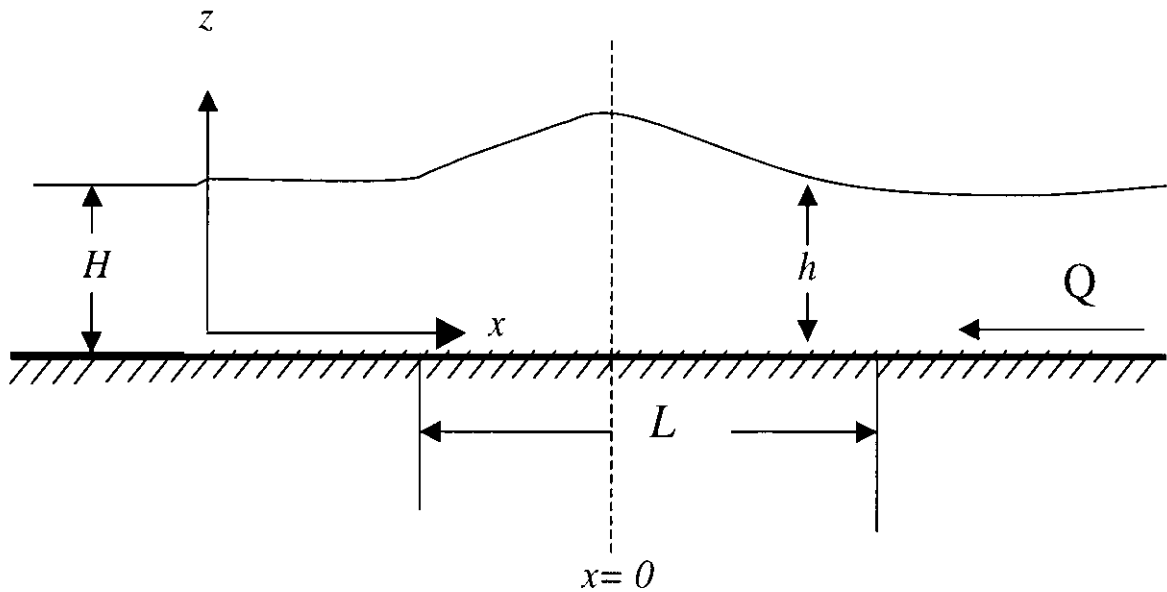


Figure 3.1 The coating profile on a flat substrate, where H is the characteristic coating thickness, L is the characteristic substrate length, and Q is the flux.

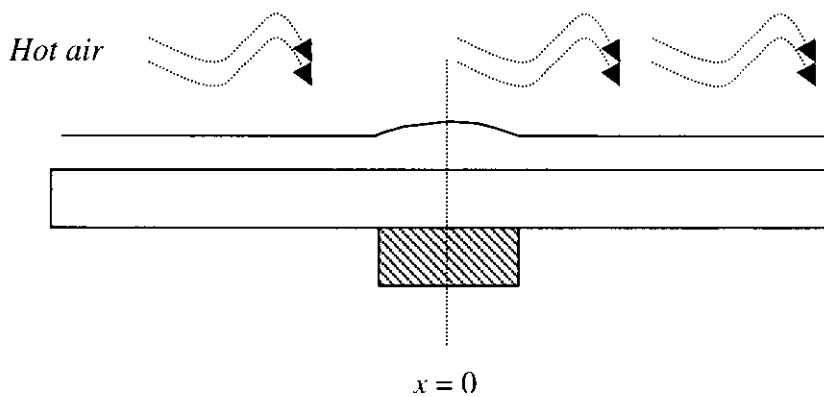


Figure 3.2 The physical situation described by the model. A coating layer is applied on the solid substrate, where a temperature-gradient is developed around the “obstacle” region.

presence of an “obstacle” underneath the coating substrate, which has a similar function as the clamp holding a fluorescent tube. This obstacle acts as a heat sink, which results in lower surface temperature in that region.

Use of the lubrication approximation is justified because the coating layer (i) is thin compared to the horizontal length ($H \ll L$), (ii) does not have abrupt changes in thickness, and (iii) is sufficiently viscous. For simplicity, the coating is assumed to be Newtonian [16]. The main feature of this model is that surface tension and viscosity are temperature dependent. The temperature profile for this study is constructed based on real conditions.

We start with the Navier-Stokes equation, which can be expressed as follows:

$$\rho \frac{Du}{Dt} = -\nabla P + \mu \nabla^2 u + \rho g \quad (3.1)$$

Neglecting inertia and gravity forces, and applying lubrication approximation theory, the resulting Navier-Stokes equation can be written as

$$\frac{\partial P}{\partial x} = \mu \frac{\partial^2 u}{\partial z^2} \quad (3.2)$$

$$\frac{\partial P}{\partial z} = 0 \quad (3.3)$$

where P is the pressure at the free surface, μ is the coating viscosity, and u is the velocity in x direction.

The mass continuity equation is

$$\frac{\partial u}{\partial x} + \frac{\partial w}{\partial z} = 0 \quad (3.4)$$

The boundary conditions can be stated as follows:

1. No-slip condition for a viscous fluid applies at the substrate boundary:

$$u = 0 \quad \text{at } z = 0 \quad (3.5a)$$

2. The fluid at the surface experiences a force along the surface towards the region of higher surface tension. The surface-tension gradient at the free surface is balanced by the shear stress in the coating, i.e.

$$\mu \frac{\partial \sigma}{\partial z} = \frac{\partial \sigma}{\partial x} \quad \text{at } z = h \quad (3.5b)$$

3. Because the local slope of the free surface is assumed to be small, an approximate form can be used for its curvature. The pressure in the coating immediately below the free surface can thus be expressed as

$$P = -\sigma \nabla^2 h \quad \text{at } z = h \quad (3.5c)$$

Integrating Equation (3.2) in the z direction twice and impose the boundary conditions in Equation (3.5) yields

$$u(x, z, t) = \frac{1}{\mu} \left(\frac{1}{2} z^2 - hz \right) \nabla P + \frac{z}{\mu} \nabla \sigma \quad (3.6)$$

Equation (3.6) indicates that the flow is driven by both the pressure and surface-tension gradients. Integrating u across the coating thickness gives the flux

$$Q(x, t) = \int_0^{h(x, t)} u(x, z, t) dz = -\frac{h^3}{3\mu} \nabla P + \frac{h^2}{2\mu} \nabla \sigma \quad (3.7)$$

Once the flux is known, the continuity relation may be used to determine the height of the coating layer, h , as a function of time. We can do so by integrating the continuity equation over the thickness of the coating layer which yields

$$\frac{\partial h}{\partial t} = -\nabla \cdot Q \quad (3.8)$$

When evaporation is present, Equation (3.8) must be modified to give

$$\frac{\partial h}{\partial t} = -\nabla \cdot Q - e(T) \quad (3.9)$$

where $e(T)$ is the temperature-dependent evaporation rate, which has a unit of cm/s.

Combining Equations (3.7) and (3.9) results in the final equation for the time-variation of coating thickness

$$\frac{\partial h}{\partial t} = -\nabla \cdot \left\{ \frac{h^3}{3\mu} \nabla (\sigma \nabla^2 h) + \frac{h^2}{2\mu} \nabla \sigma \right\} - e(T) \quad (3.10)$$

where μ and σ are functions of temperature.

To form a complete model, expressions for viscosity, surface tension, and evaporation rate as functions of temperature are required:

$$\mu(T) = \mu_0 \left(1 - \frac{T}{T_c} \right) \quad (3.11a)$$

$$\sigma(T) = \sigma_0 \left(1 - \frac{T}{T_c} \right) \quad (3.11b)$$

$$e(T) = e_0 \left(\frac{T + C}{T_c} \right) \quad (3.11c)$$

where μ_0 is initial viscosity, σ_0 is reference surface tension, e_0 is reference evaporation rate, and T_c is the critical temperature of pure liquid.

Equations (3.11a) to (3.11c) are empirical, which are written in such a way that the viscosity and surface tension decrease with increasing temperature whereas the evaporation rate increases with the increasing temperature. The constant, C , in Equation (3.11c) varies from 2 to 42, depending on the temperature variation. It is simply an arbitrary constant used to study the effect of doubling evaporation rate on coating thickness (see chapter 4).

3.2 Dimensionless model

It is convenient to nondimensionalise the equations before attempting a numerical solution. We define the dimensionless quantities as follows:

$$\begin{aligned} x &= Lx^* \\ y &= Hy^* \\ t &= \bar{T}t^* \\ h &= Hh^* \\ P &= P_0P^* \end{aligned} \quad (3.12)$$

Table 3.1 Base properties of the coating used for simulation (taken from ref. [8]).

<i>Properties, symbol</i>	<i>Value</i>
Initial coating thickness, H	30 μm
Horizontal length scale, L	1.25 cm ^x
Reference surface tension, σ_0	30 dyne/cm
Minimum surface tension, σ_∞	22 dyne/cm
Initial coating viscosity, μ_0	2 Poise ⁺
Initial drying rate, e_0	2×10^{-6} cm/s
Reference pressure, P_0	0.6 dyne/cm ² *

* The reference pressure is based on the reference tension, σ_0 .

+ This value is taken from ref [21].

x This value corresponds to the defects found on a fluorescent lamp.

Here H is taken as the thickness of the initial undisturbed layer. The reference for length along the substrate is L . The dimensionless surface tension σ^* is defined as

$$\sigma(T) = (\sigma_0 - \sigma_\infty)\sigma^*(T) + \sigma_\infty \quad (3.13)$$

Viscosity is nondimensionalised by defining

$$\mu = \mu_0\mu^*$$

Making the above substitutions we find that this occurs if \bar{T} is chosen to be the Orchard leveling time [17]:

$$\bar{T} = \frac{3\mu_0 L^4}{\sigma_0 H^3} \quad (3.15)$$

Re-writing Equation (3.9) in dimensionless form, in one dimension, yields

$$\frac{\partial h^*}{\partial t^*} = -\frac{\partial Q^*}{\partial x^*} - E(T) \quad (3.16)$$

where

$$Q^* = \frac{h^{*3}}{\mu^*} \frac{\partial}{\partial x^*} \left(\frac{\partial^2 h^*}{\partial x^{*2}} \right) + A \frac{h^{*2}}{\mu^*} \frac{\partial \sigma}{\partial x} \quad (3.17)$$

In Equation (3.17), the variation of σ in the pressure-gradient term has been neglected, since it is negligible compared to the surface-tension gradient term when $H \ll L$, as discussed by Eres et. al. [7]. The aspect ratio is defined as

$$A = \frac{3}{2} \frac{\sigma_0 - \sigma_\infty}{\sigma_0} \left(\frac{L}{H} \right)^2 \quad (3.18)$$

This aspect ratio reflects the contribution of surface-tension gradient to the total flux, relative to leveling. A large ratio results when the coating layer is very thin compared to the horizontal scale of the defect.

The evaporation parameter E is a dimensionless quantity defined as

$$E = \frac{\bar{T}e_0}{H} \quad (3.19)$$

Typical evaporation rates can vary from 2×10^{-9} cm/s to 2×10^{-5} cm/s [18], while initial coating viscosities usually are in the range between 1 P to 10 P [19].

The boundary and initial conditions for solving Equation (3.16) are as follows:

(1) Initial condition: $h^* = 1$ for all x^* at $t^* = 0$.

(2) Because of symmetry:

$$\frac{\partial h^*}{\partial x^*} = 0 \quad \text{at} \quad x^* = 0 \quad (3.20a)$$

(3) Far from the location of the temperature gradient, the disturbance should have no effect, and there is no flow of coating. Thus we impose the following condition:

$$\frac{\partial h^*}{\partial x^*} = 0, \quad Q^* = 0 \quad \text{at} \quad x^* = L_\infty \quad (3.20b)$$

3.3 Derivation of Discretization Equations

The finite difference method is used to solve the differential equation numerically. For convenience, in the remainder of this chapter, the superscript “*” will be omitted from dimensionless quantities, except where necessary.

The solution domain, $0 \leq x \leq L_\infty$, is divided into $N - 1$ equally spaced intervals, each of length Δx . The derivatives are evaluated using forward differencing technique, i.e.

$$h^j_{xxxx}(i) = \frac{h^j(i+4) - 4h^j(i+3) + 6h^j(i+2) - 4h^j(i+1) + h^j(i)}{(\Delta x)^4}$$

$$h^j_{xxx}(i) = \frac{h^j(i+3) - 3h^j(i+2) + 3h^j(i+1) - h^j(i)}{(\Delta x)^3}$$

$$h^j_{xx}(i) = \frac{h^j(i+2) - h^j(i+1) + h^j(i)}{(\Delta x)^2}$$

$$\begin{aligned}
h^j_x(i) &= \frac{h^j(i+1) - h^j(i)}{\Delta x} \\
\sigma_{xx}(i) &= \frac{\sigma(i+2) - \sigma(i+1) + \sigma(i)}{(\Delta x)^2} \\
\sigma_x(i) &= \frac{\sigma(i+1) - \sigma(i)}{\Delta x} \\
\mu_x(i) &= \frac{\mu(i+1) - \mu(i)}{\Delta x}
\end{aligned} \tag{3.21}$$

where superscript j denotes the j^{th} time step, index i denotes the i^{th} grid points, and subscripts x refers to the order of derivative with respect to x . For last four spatial grid points, the derivatives were evaluated using backward differencing:

$$\begin{aligned}
h^j_{xxx}(i) &= \frac{h^j(i) - 4h^j(i-1) + 6h^j(i-2) - 4h^j(i-3) + h^j(i-4)}{(\Delta x)^4} \\
h^j_{xx}(i) &= \frac{h^j(i) - 3h^j(i-1) + 3h^j(i-2) - h^j(i-3)}{(\Delta x)^3} \\
h^j_x(i) &= \frac{h^j(i) - 2h^j(i-1) + h^j(i-2)}{(\Delta x)^2} \\
h^j_x(i) &= \frac{h^j(i) - h^j(i-1)}{\Delta x}
\end{aligned} \tag{3.22}$$

The finite-difference form of Equation (3.10) is

$$\frac{h^{j+1}(i) - h^j(i)}{\Delta t} = - \left\{ \begin{aligned} & \left[\frac{(h^j(i))^3}{\mu(i)} \left(h_{xxx}^j(i+4) \right) + 3 \frac{(h^j(i))^2}{\mu(i)} \left(h_{xx}^j(i+3) \right) \left(h_x^j(i+1) \right) - \frac{(h^j(i))^3}{\mu^2(i)} \left(h_{xx}^j(i+2) \right) \right] \\ & \left[\left(\mu_x(i+1) + A \right) \left[\frac{(h^j(i))^2}{\mu(i)} \left(\sigma_{xx}(i+2) \right) + 2 \frac{h^j(i)}{\mu(i)} \left(\sigma_x(i+1) \right) - \frac{(h^j(i))^2}{\mu^2(i)} \left(\sigma_x(i+1) \right) \right] \right. \\ & \left. \left(\mu_x(i+1) \right) \right] \end{aligned} \right\} \tag{3.23}$$

A fully explicit scheme was used throughout this study mainly due to its relative ease of implementation compared with other schemes. However, it should be noted that, in fully explicit scheme, Δt and Δx are constrained by the stability criterion [20].

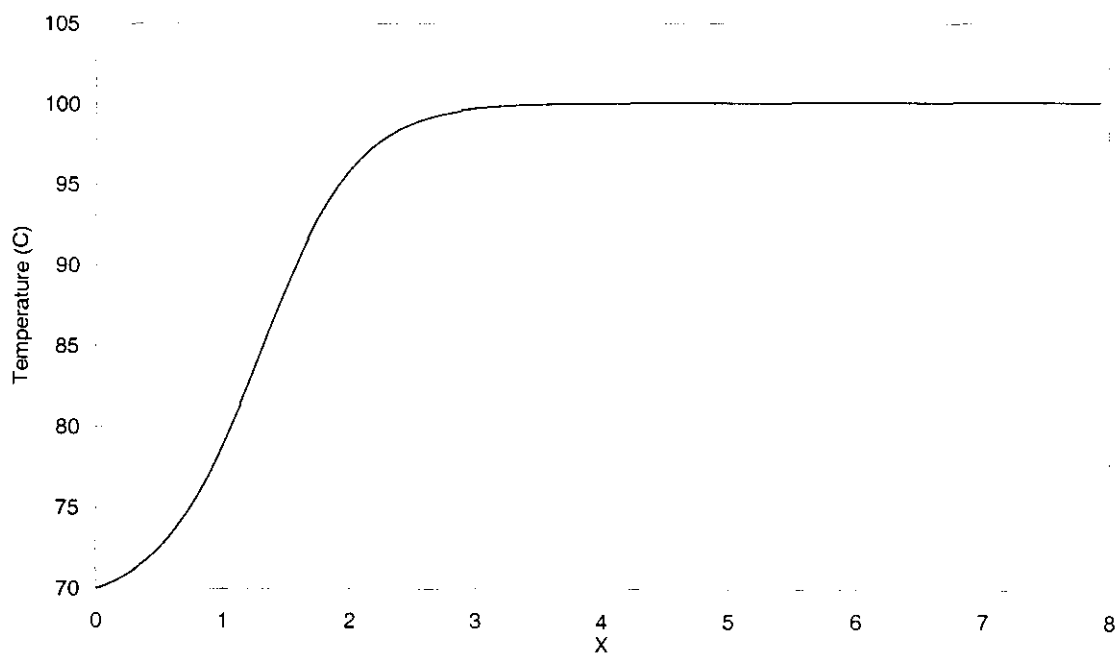


Figure 4.1 Temperature distributions over dimensionless axial x -direction.

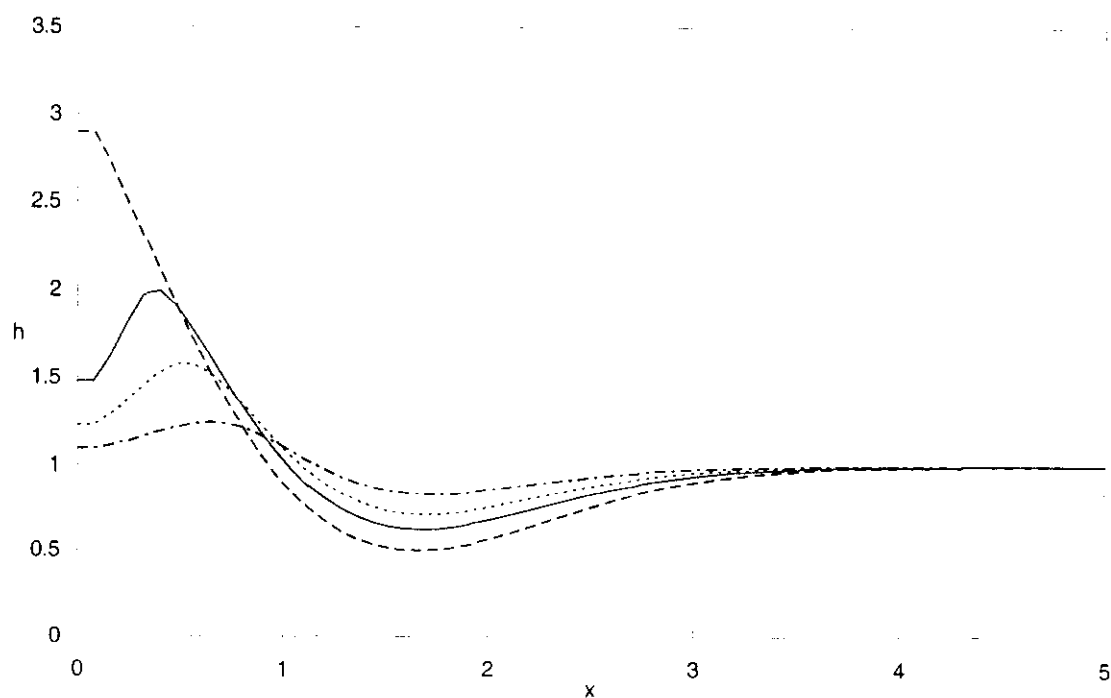


Figure 4.2 Time variation of dimensionless coating thickness. Dash line: $t = 500$ s, solid line: $t = 300$ s, dotted line: $t = 200$ s, and dash-dotted line: $t = 100$ s.

Figure 4.2 shows the variation of coating thickness in the temperature-gradient region, which would be detected as a coating defect (see Figure 4.1). The coating material in the warmer region ($T = 100^\circ\text{C}$, lower surface tension) is drawn to the cooler region (70°C , higher surface tension). The initial ($t = 100$ s) variations in coating thickness are small, but they gradually become more pronounced. This build-up of coating material towards the centerline can be understood by analysing the various fluxes involved.

Figure 4.3 depicts a comparison between the flux driven by surface-tension gradient, Q_{stg} , and the flux due to pressure gradient, Q_{pg} . As shown in the figure, the magnitude of Q_{stg} is much larger than that of Q_{pg} , which indicates that surface-tension gradient is the dominant driving forces for defect formation. The flux due to pressure gradient, Q_{pg} , is shown in more details in Figure 4.4. At time $t = 50$ s, Q_{pg} is almost zero, but its magnitude increases gradually with time. At $t = 300$ s, Q_{pg} is negative between $x = 0$ to $x \approx 0.24$, but it is positive between $x \approx 0.24$ and $x \approx 0.9$. This behaviour implies that the pressure gradient can have opposing effect on defect growth.

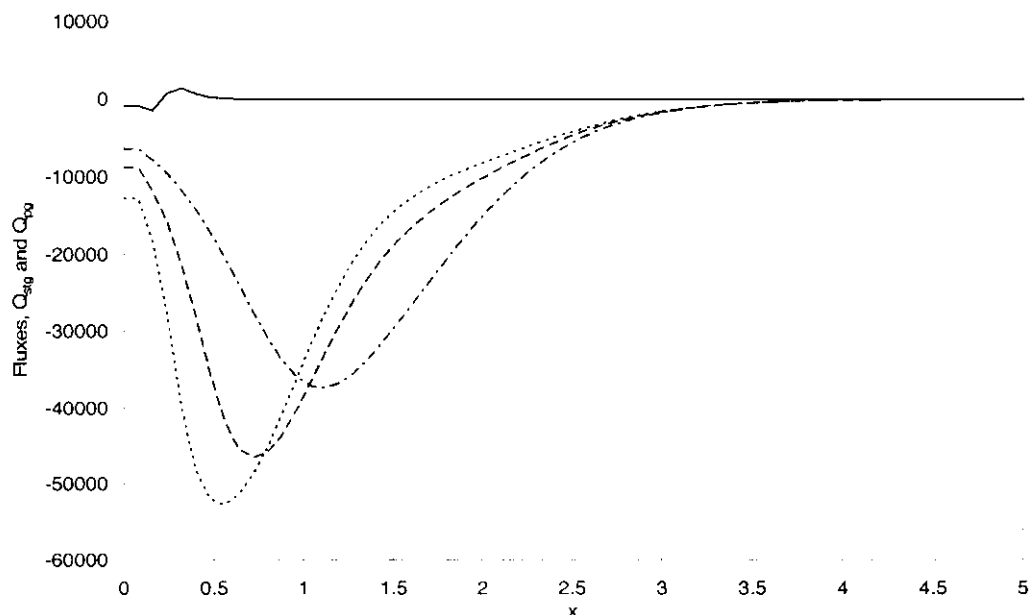


Figure 4.3 Distribution of fluxes due to surface-tension gradient (Q_{stg}) and pressure gradient (Q_{pg}). Solid line: Q_{pg} at $t = 300$ s, dotted line: Q_{stg} at $t = 300$ s, dash line: Q_{stg} at $t = 200$ s, and dash-dotted line: Q_{stg} at $t = 50$ s.

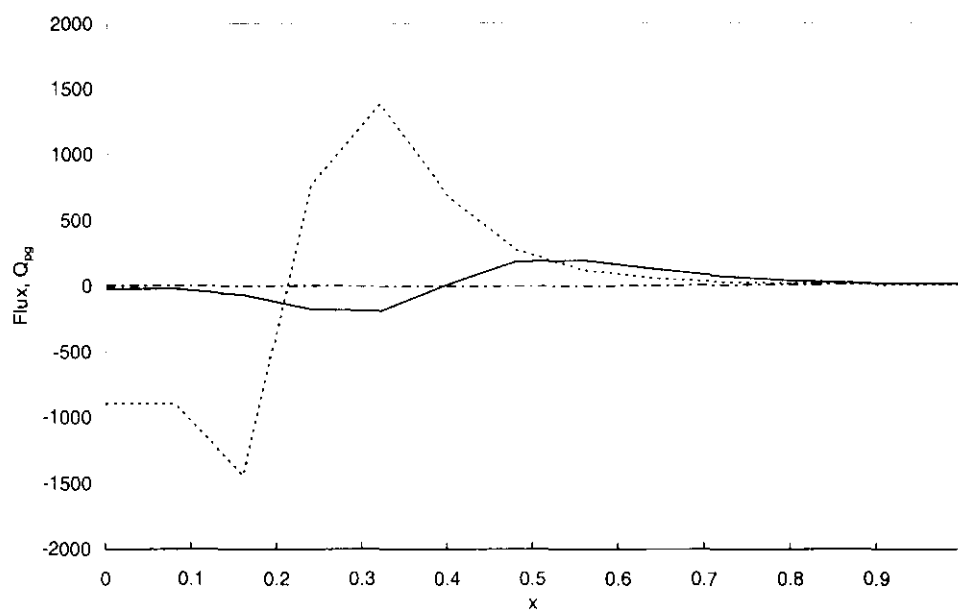


Figure 4.4 Flux due to pressure gradient. Dotted line: $t = 300$ s, solid line: $t = 200$ s, and dash-dotted line: $t = 50$ s.

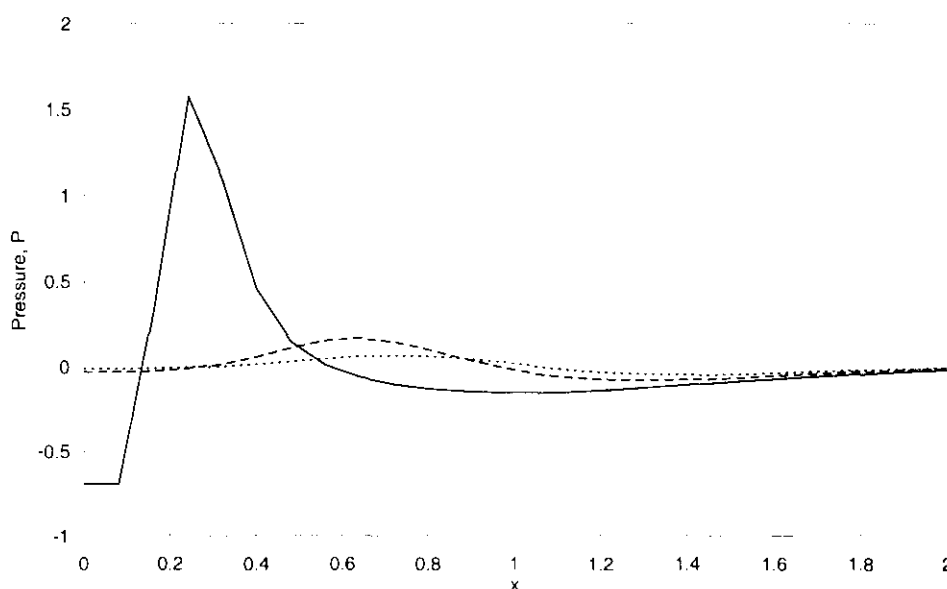


Figure 4.5 Dimensionless pressure distributions at free surface at different times. Solid line represent $t = 300$ s, dashed line represent $t = 100$ s and dotted line represent $t = 50$ s.

To understand this effect better, the pressure at the coating free surface is plotted in Figure 4.5. It should be noted that the pressure at the free surface depends only on the local surface tension and the free surface curvature. Initially, the pressure gradient at the free surface is small, which means that Q_{pg} is negligible (see Figure 4.4). The magnitude of pressure gradient gradually increases with time. At $t = 300$ s the pressure gradient is negative between $x = 0$ and $x \approx 0.24$, corresponding to the negative Q_{pg} in the same region. From $x = 0.24$ to $x \approx 1$, the pressure gradient is positive, which corresponds to the positive Q_{pg} (again see Figure 4.4).

4.1.3 Data analysis

To gain a better insight into the mechanisms of defect formation, the numerical results are further analysed for variations in peak location, peak height, defect growth rate, and spreading of the defect.

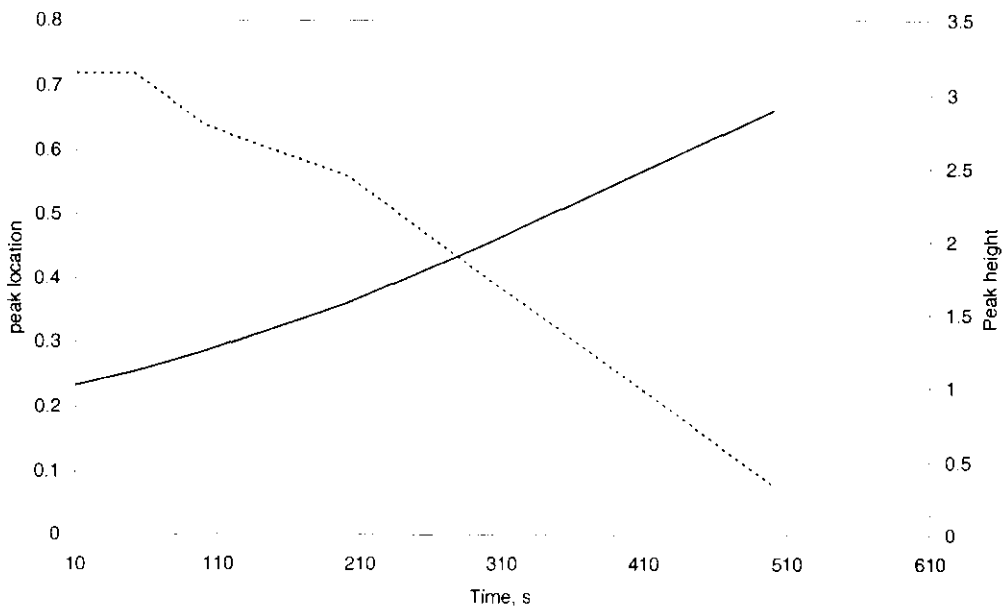


Figure 4.6 Variation of peak height and peak location. The solid and dotted lines represent the peak height and peak location, respectively.

Figure 4.6 shows that the variation of peak height and peak location at different times. Note that the peak height increases with time, but its movement behaves differently. The

peak initially remains stationary until $t = 50$ s, then gradually migrates towards the centerline. The linear relationship between peak height and time indicates that the peak grows at a constant rate from $t = 10$ s to $t = 500$ s. Peak location plotted against time, indicates that, surface-tension gradient only drive the flow until $t = 300$ s. However, the pressure gradient has insignificant effect at the beginning, but it becomes important with increases of time i.e. $t = 300$ s.

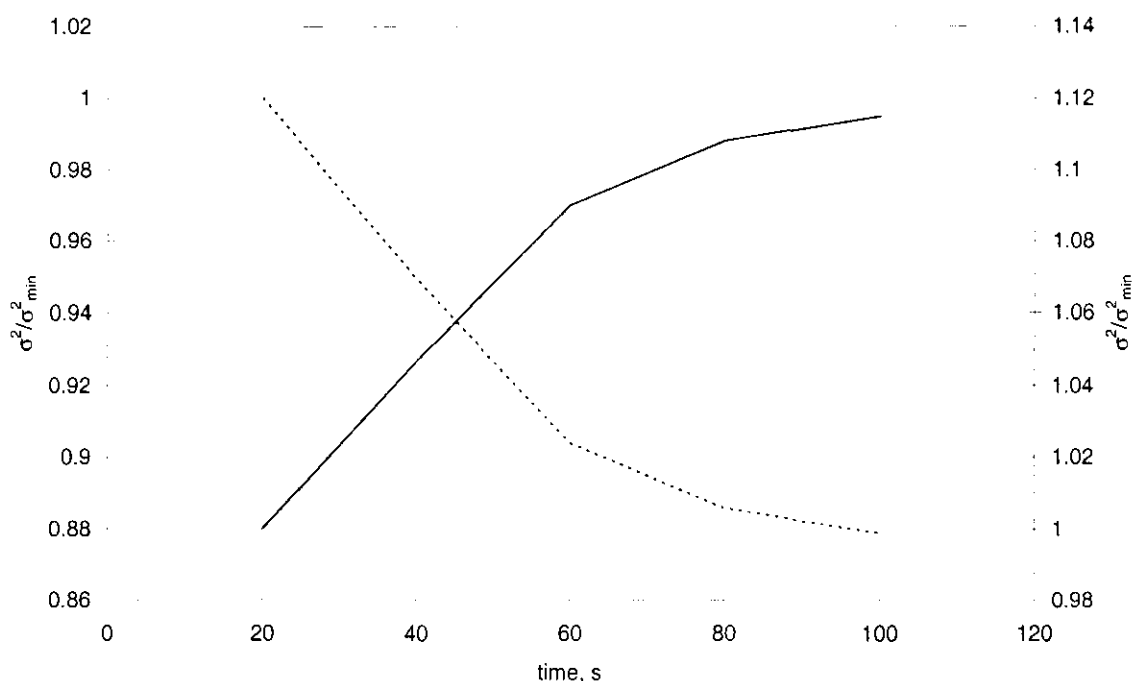


Figure 4.7 The peak and trough variances at different times. The solid line and dotted line represent the trough and peak, respectively.

Figure 4.7 shows the spreading of the peak and trough of the defect. The spreading is quantified by the relative variance of the height distribution, using $t = 20$ s as a reference time. Note that, to simplify the analysis, the temperature profile was shifted away from the centerline so that no significant temperature gradient exists at the centerline (see Figure 4.8). The relative spreads of the peak regions decrease gradually until they reach the centerline whereas the troughs widen as time increases.

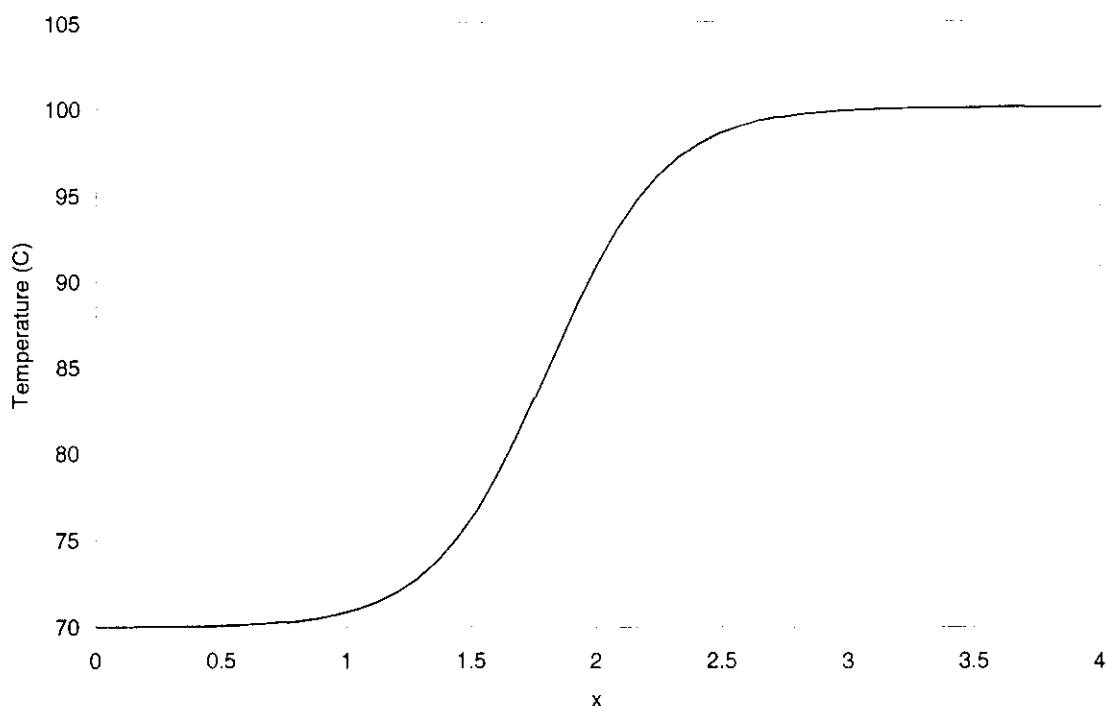


Figure 4.8 Temperature profile used in studying defect spreading.

4.2 Effect of evaporation rate

To investigate the effect of evaporation rate on defect formation, the evaporation rate, $e(T)$, was varied from 5.38×10^{-7} to $1.2 \times 10^{-5} \text{ cm s}^{-1}$ depending on the temperature variation as explained in chapter 3.

As shown in Figure 4.9, a 10-fold increase in evaporation rate reduces the peak by 50 % and the trough spread by 20 %. In addition, a high evaporation rate also causes the coating to level off. At $x = 2$, the trough is levelled off due to the higher evaporation rate in the region than preceding region. This can be understood as the evaporation rate increased with temperature as depicted in Figure 4.10.

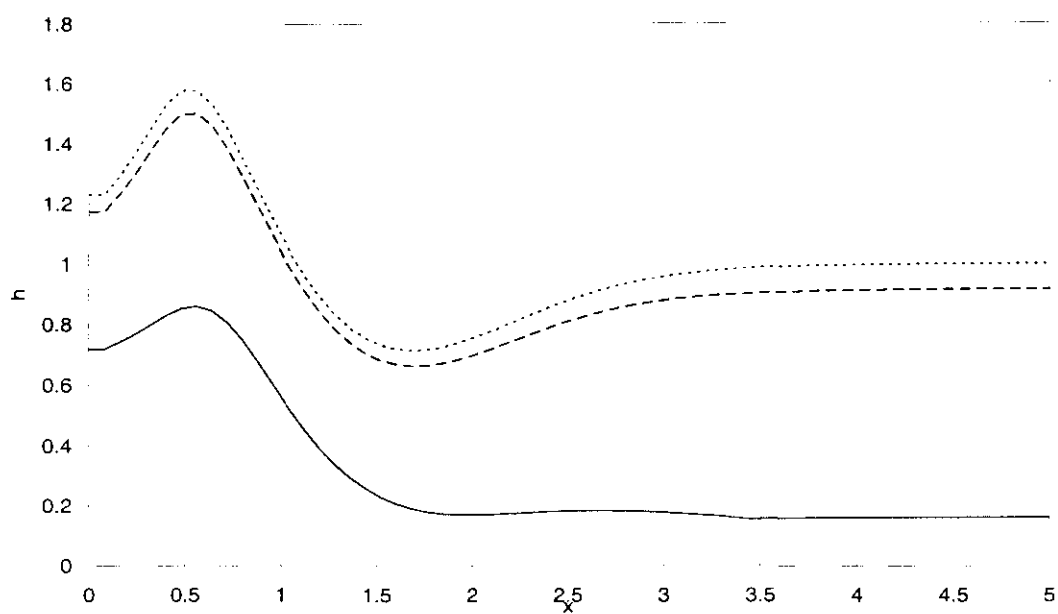


Figure 4.9 Coating thickness profile at $t = 200$ s, effect of evaporation rate. Solid line: $E = 10e(T)$, dashed line: $E = e(T)$, and dotted line: $E = 0$.

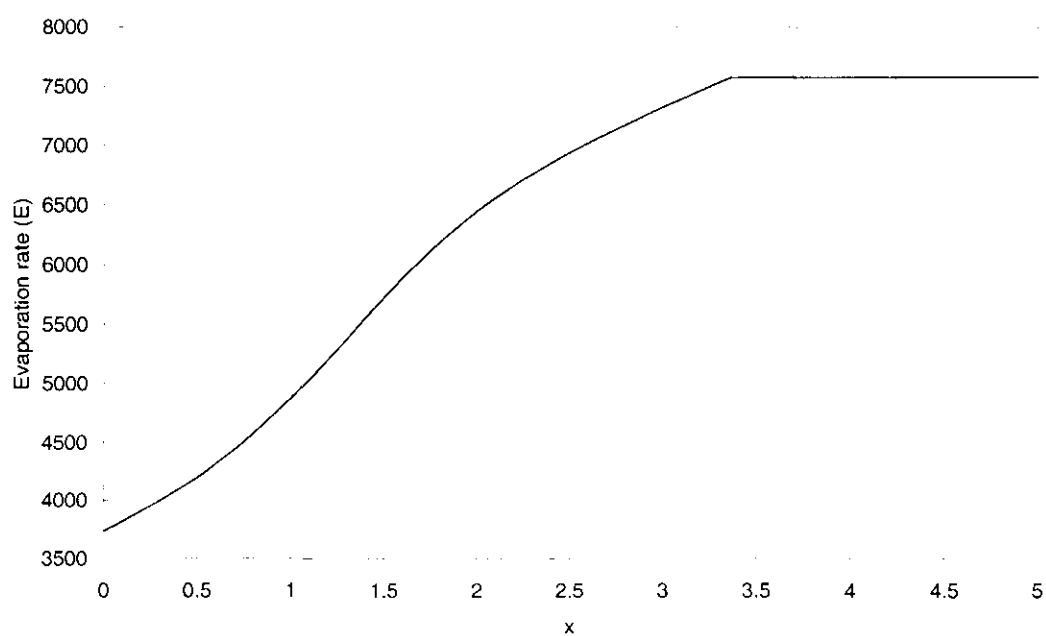


Figure 4.10 Evaporation rate profile. Evaporation rate increases with dimensionless x -direction until it reaches $x \approx 3.5$.

4.2 Effect of viscosity

Three different viscosities were selected in this analysis: 2, 0.5 and 0.1 Poise. As described in Equation (3.11a), viscosity decreases with increasing temperature. The effect of viscosity on defect growth is depicted in Figure 4.11. As viscosity decreases, the defect becomes more pronounced and the peak also moves faster towards the centerline.

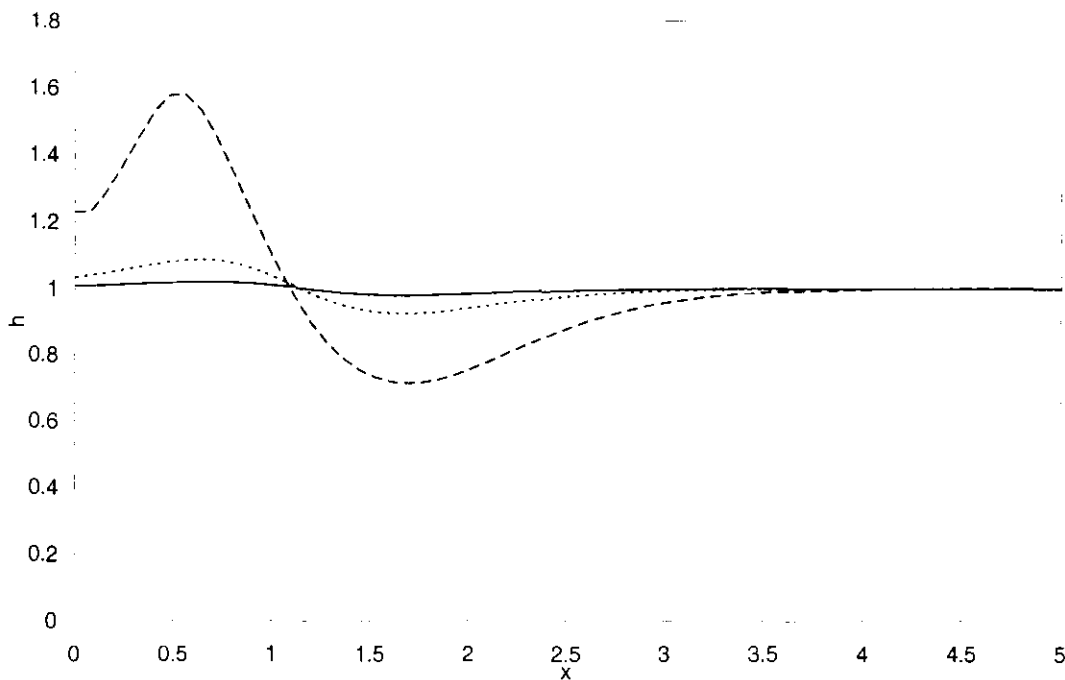


Figure 4.11 Coating thickness profiles at $t = 10$ s showing the effect of viscosity. Solid line: 2 P, dotted line: 0.5 P, and dash line: 0.1 P.

Figure 4.12 shows that the defect formation time varies linearly with increasing viscosity. The defect formation time is taken as the time required for the peak height to reach approximately 2.44. The highest rate of growth (0.04 s^{-1}) was found at lower viscosity (0.1 P), between $t = 6$ and 8 s. As shown in Figure 4.13, the time variations in peak height and its location display similar pattern at different viscosities.

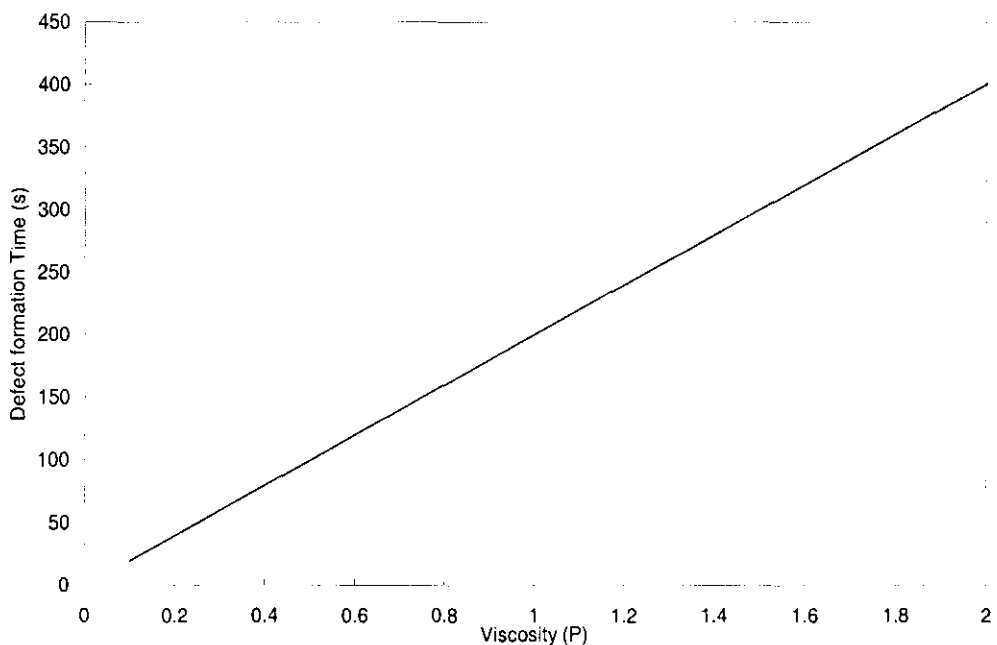
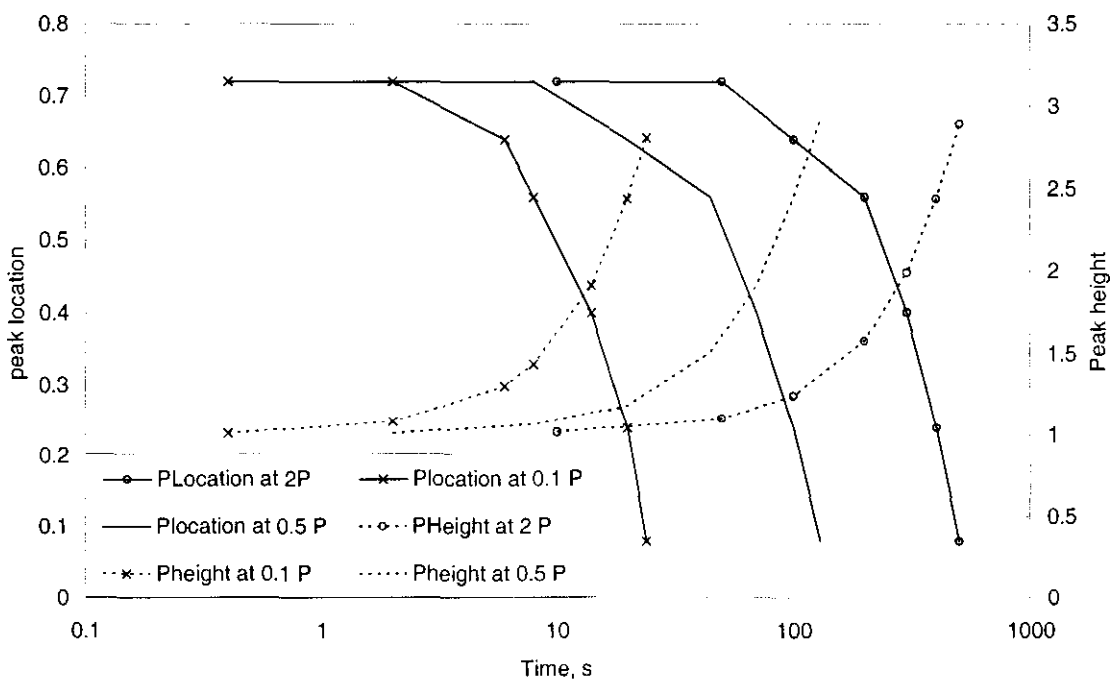


Figure 4.12 The linear relation between defect formation time and viscosity. Defect formation time is the time required for the peak height to reach approximately 2.44.



PUSAT SUMBER MAKLUMAT
UNIVERSITI TEKNOLOGI PETRONAS

Figure 4.13 Defect growth behaviour at different viscosities.

4.3 Effect of temperature gradient

In this analysis, different temperature profiles were imposed on the coating surface (see Figure 4.14):

1. Base-case temperature profile.
2. Case 2: total temperature difference doubled to 60 °C .
3. Case 3: temperature profile with lower gradient than base case.

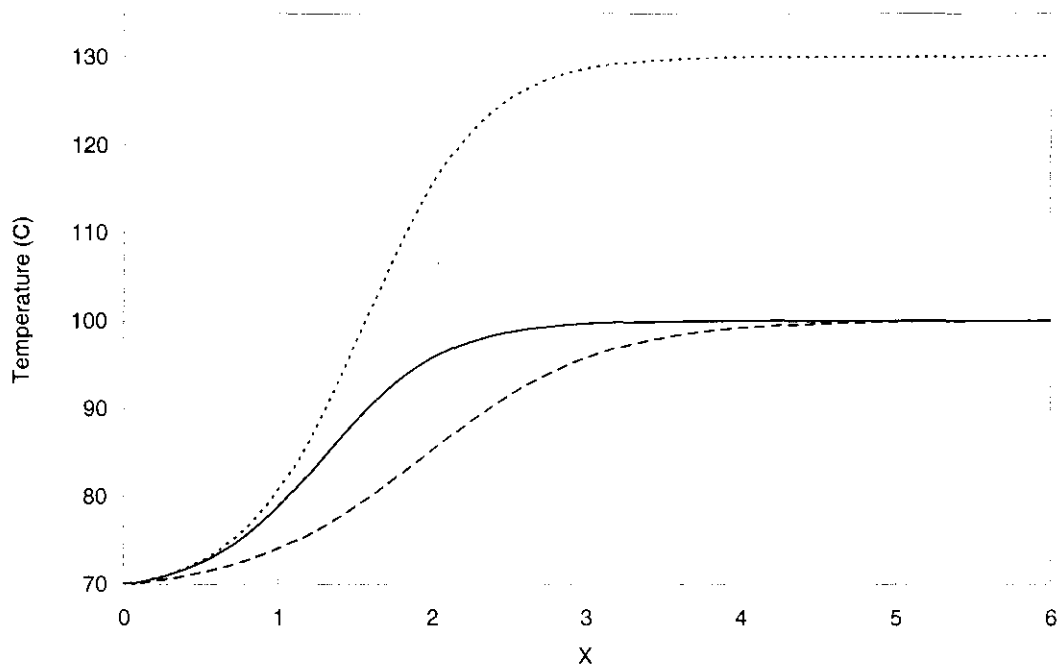


Figure 4.14 Temperature profiles for studying the effect of temperature gradient. Solid line: base case, dotted line: case 2, and dash line: case 3. All profiles were taken at $t = 10$ s.

Figure 4.15 shows the effects of temperature gradient on defect formation. Case 2 shows that, with a larger gradient, the peak height and spread of the defect increase by 123 % and 16 %, respectively, compared to the base case. The peak due to the larger temperature gradient seems to move farther away from the centerline. The trough of the

defect also becomes deeper compared to the base case. This behaviour is due to a higher surface tension gradient, which was explained in a previous section. Comparing case 3 to the base case (see Figure 4.14), there is a 44 % reduction in peak height, but the spread of defect increases by 125 %.

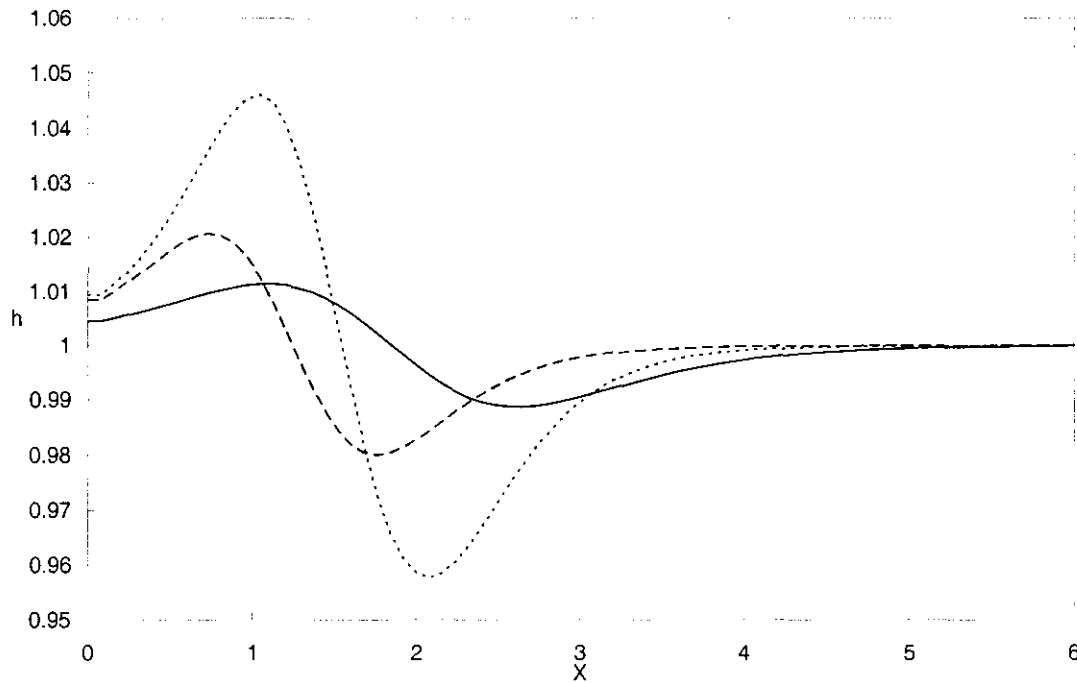


Figure 4.15 Effect of temperature gradient on coating thickness at $t = 10$ s. Dash line: base case, dotted line: case 2, and solid line: case 3.

4.4 Effect of surface tension

As explained in chapter 3, surface tension is a function of temperature. In this analysis, we vary the surface tension by manipulating the exponent, n , in the following equation:

$$\sigma(T) = \sigma_0 \left(1 - \frac{T}{T_c} \right)^n$$

From Figure 4.16, we can see that surface tension has a significant effect on defect growth. It is observed that the peak shifts closer to the centerline after certain time. The peak and trough are reduced by 38 % and 35 %, respectively, for $n = 0.5$. For $n = 2$, both peak and trough are increased by 25 %.

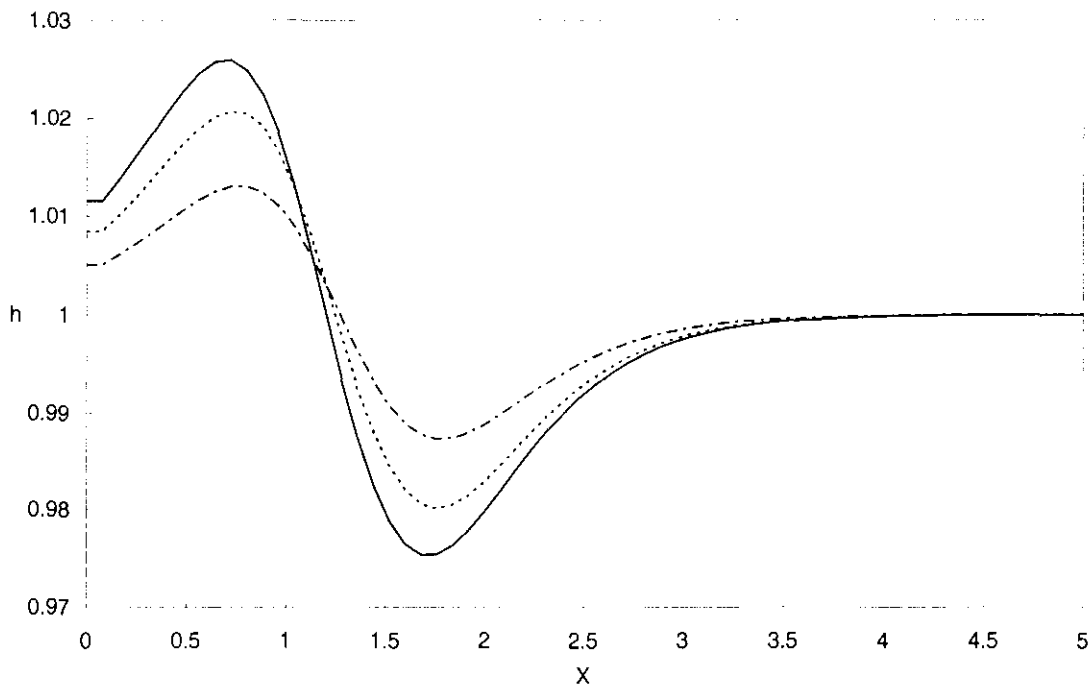


Figure 4.16 Effect of surface tension on coating thickness. Solid line: $n = 2$, dotted line: $n = 1$ (base case), and dash-dotted line: $n = 0.5$.

4.5 Discussion

From the base-case results, the variation of coating thickness occurs only in the temperature-gradient region. The coating material is drawn towards the centerline, which is from the region of lower surface tension to the region higher surface tension. In the flux analysis, the magnitude of the flux due to surface-tension gradient, Q_{stg} , is far larger than that due to pressure gradient, Q_{pg} . Q_{pg} is negative between $x = 0$ and $x \approx 0.24$ and

positive between $x = 24$ and $x \approx 1$. The pressure gradient is negative between $x = 0$ and $x \approx 0.24$ and positive between $x = 24$ and $x \approx 1$. Based on the pressure-gradient results, at $t = 50$ s and $t = 100$ s, the pressure gradient is zero in that time range. In the data analysis results, the peak remains stationary until $t = 50$ s, then gradually decreases towards the centerline. The peak height increases with time in the range between $t = 0$ to $t = 500$ s. In the spreading analysis result, the trough gradually widens with time while the peak sharpens with time in the range between $t = 0$ and $t = 80$ s.

Parametric studies show that a 10-fold increase of evaporation rate reduces the peak height and trough by 50 % and 20 %, respectively. Viscosity has a significant effect on defect growth. At $\mu = 0.1$ P the peak increases significantly compared to $\mu = 2$ P. From this analysis, a higher viscosity can substantially slow down defect growth. The viscosity acts as a resistant force against defect formation. Three cases were studied to understand the effect of temperature on defect formation. A small reduction in temperature gradient induces a significant reduction in both peak height and trough of the defect. The peak and trough were reduced by 38 % and 35 %, respectively for $n = 0.5$ (surface tension increased), but they were increased by 25 % for $n = 2$.

From the above discussions, all the parameters studied have an effect on defect formation. Among these parameters, temperature gradient and viscosity seem to have the largest influence. Temperature gradient can be controlled using proper selection of heating power and material used for the clamp i.e. fluorescent-lamp industry.

Chapter 5

CONCLUSIONS

A mathematical model has been developed to describe the effect of temperature-induced surface-tension gradient in coating processes. The one-dimensional rectangular model was derived based on the established Navier-Stokes equation. By implementing a series of parametric studies, the following conclusions can be made:

1. Temperature-induced surface-tension gradient plays a major role in the behaviour of defect growths in a drying coating. As mentioned earlier, defects such as “dark lines” are often found in fluorescent lamps. Thus, based on the results of this study, it is highly probable that this type of defect is caused by temperature-induced surface-tension gradients. However, other factors, including surfactant-induced surface tension gradient, must also be considered.
2. The peak of the defect grows linearly with time in the range between $t = 10$ and 500 s.
3. Defect formation time varies linearly with increasing coating viscosity within the range 0.1 P to 2 P. Evaporation rate can reduce the height and spread of the defect.
4. According to the parametric studies, temperature gradient, viscosity, surface tension and evaporation rate have an influence on the defect formation. The temperature gradient seems to have the largest influence compared to other parameters, followed by viscosity. Proper selection of heating power and the material of the clamp (i.e. the fluorescent lamp industry) may be able to reduce the temperature gradient, thus reducing the defect caused surface-tension gradient.

5. The effect of pressure-gradient is small compared to that of surface-gradient gradient. Surface-tension gradient is the largest driving force in defect formation. The pressure gradient may act as an opposing factor.

Chapter 6

LIMITATIONS OF MODEL AND FUTURE WORKS

Instead of focusing on the usefulness of the model, it will be beneficial to identify its limitations, so that the model can be interpreted in a more sensible manner and can be applied in a successful way.

6.1 Model limitations

The limitations of the model are as follows:

- (1) In this study, the effect of gravitational force was neglected in the pressure term. In the case of cratering, this assumption may be valid because the size of the crater is very small, which implies that the Bond Number, \mathbf{Bo} , is sufficiently small for the gravitational effects to be neglected. \mathbf{Bo} is defined as the relative importance between the gravitational and surface tension effect. The gravitational effect can be neglected when the $\mathbf{Bo} \ll 1$. However, in this case, the defect size is quite large, and gravitational effects may need to be considered.
- (2) As stated earlier, a coating is usually a multi-component mixture. A one-component model is not able to simulate the full range of behaviour. For example, a concentration gradient may develop between two components, which will also induce surface-tension gradient, if evaporation takes place.
- (3) Typically, the coating materials contain a surfactant as a substance, which lowers the surface tension. The surfactant effect was neglected in this work. In reality, surfactant also plays a major role in the increase in wettability in coating processes by lowering surface tension. It would be more realistic to include surfactant in modeling.

- (4) It is important to have an experimental data to backup the numerical results. This can be done by conducting the experiments by ourselves or using others similar work to validate the numerical results.
- (5) Viscosity, surface tension, and evaporation rates are function of temperature. These relationships were based on empirical assumptions. To be more realistic, these relationships should be based on the experimental results.

6.2 Future works

As hinted in the limitation of the model, the mathematical aspects should be the top priority and be a backbone for future work. The gravitational and surfactant effects should be incorporated, which will make the simulation more realistic. Gravitational effects should not pose any problem, since all the basic model equations will remain the same, except for the pressure term in the flux equation. To account for the effects of surfactants, however, a new set of equation must be formulated. This can be done by assuming that the surfactant is transported along the surface due to fluid motion and molecular diffusion. As mentioned before, coatings are often multi-component mixtures. Thus, a better model should include at least two components of coating materials, such as the solvent and resin as volatile and non-volatile components, respectively.

REFERENCES

- [1] National Paint & Coatings Association. Industry Info, 1999, www.paint.org/ind_info/ [Retrieved: October 13, 2002].
- [2] Cohen, E.D.; Gutoff, E.B. Modern Coating and Drying Technology, Vol.1, Interfacial Engineering Series, VCH Publishers, Inc., New York, 1992.
- [3] Rosen, M.J. Surfactants and Interfacial Phenomena, Wiley, New York, 2nd ed., 1998.
- [4] Robert, A.A. Physical Chemistry, Wiley, 6th ed., 1983.
- [5] Weh, L.; Linde, H. Kraterförmige Oberflächenstörungen in Anstrichfilmen, verursacht durch Silikonölzusätze (Crater-shaped defects of paint films, caused by addition of silicon oil), *Plaste und Kautschuk*, 20(11):849-860, November 1973.
- [6] Overdiep, W.S. "The leveling of paints," *Progress in Organic Coatings*, 14:159-175, 1986.
- [7] Eres, M.H.; Weidner, D.E.; Schwartz, L.W. "Three-dimensional direct numerical simulation of surface-tension gradients effects on the leveling of an evaporating multicomponent fluid," *Langmuir*, 14(4):1849-1871, 1991.
- [8] Evans, P. L.; Schwartz, W. L ; Roy, R. V. "Mathematical model for crater defect formation in a drying paint layer," *J. Colloids Interface Sci.*, 227:191-205, March 2000.
- [9] Carles, P.; Cazabat, A. M.; Heslot, F.; Troian, S. M. "Spreading in presence of surface tension gradients," *Phy. Chem. Colloids Interfaces in Oil Production*, 161-164, 1992.

- [10] Heiple, C. R.; Roper, J. R. "Mechanism for minor element effect on GTA fusion zone geometry," *Weld. Res. (Miami)*, 61(4):97-102, April 1982.
- [11] Oreper, G. M.; Szekely, J. "Heat-flow and fluid-flow phenomena in weld pools," *J. Fluid Mech.*, 147:53-79, October 1984.
- [12] Zacharia T.; David, S. A. "Heat and fluid flow in welding," in *Mathematical Modeling of Weld Phenomena*, Cerjak, H. and Easterling, K. E. (eds), pp.3-23, The Institute of Materials, London, 1993.
- [13] Lei, Y. P.; Murukawa H. Shi, Y. W.; Li, X. Y. "Numerical analysis of the competitive influence of Marangoni flow and evaporation on heat surface temperature and molten pool shape in laser surface remelting," *Comp. Materials Sci.*, 21:276-290, 2001.
- [14] Blunk, R. H. J.; Wilkes, J. O. "Computational analysis of surface-tension-driven coating defect flow," *AIChE J.*, 47(4):779-789, April 2001.
- [15] Blunk, R. H. J.; Wilkes, J. O. "Surface-tension driven flows of coatings: bondline readout formation," *J. Coat. Technol.*, 73(918):63-71, July 2001.
- [16] Deen, W. M. *Analysis of Transport Phenomena*, Oxford, New York, 1998.
- [17] Orchard, S.E. "On surface leveling in viscous liquids and gels," *Applied Scientific Research Section A*, 11:451-464, 1962.
- [18] Stratta, J. J.; Dillon, P.W.; Semp, R. H. "Evaporation of organic cosolvents from water-borne formulations: theory, experimental study, computer-simulation," *J. Coat. Technol.*, 50(647):39-47, December 1978.
- [19] Guttoff, E. B.; Cohen, E. D. *Coating and Drying Defects: Troubleshooting Operating Problems*, SPE monographs, Wiley-Interscience, New York, 1995.

- [20] Carnahan, B.; Luther, H. A.; Wikes, J. O. *Applied Numerical Methods*, Wiley, New York, 1969.
- [21] Orchard, S.E. "On surface leveling in viscous liquids and gels," *Applied Scientific Research Section A*, 11:451 – 464, 1962.